Energy 239 (2022) 122127

Contents lists available at ScienceDirect

Energy

journal homepage: www.elsevier.com/locate/energy

Annular thermoelectric generator performance optimization analysis based on concentric annular heat exchanger

Wenlong Yang [a, 1], WenChao Zhu [a, b, 1], Yang Li [a], Leiqi Zhang [c], Bo Zhao [c], Changjun Xie [a, b, *], Yonggao Yan [d], Liang Huang [a]

[a] School of Automation, Wuhan University of Technology, Wuhan, 430070, China
[b] Hubei Key Laboratory of Advanced Technology for Automotive Components, Wuhan University of Technology, Wuhan, 430070, China
[c] State Grid Zhejiang Electric Power Research Institute, Hangzhou, 310014, Zhejiang Province, China
[d] State Key Laboratory of Advanced Technology for Materials Synthesis and Processing, Wuhan University of Technology, Wuhan, 430070, China

ARTICLE INFO

Article history:
Received 4 May 2021
Received in revised form
3 August 2021
Accepted 19 September 2021
Available online 24 September 2021

Keywords:
Annular thermoelectric generator
Concentric annular exchanger
Waste heat recovery
Size optimization

ABSTRACT

In order to increase the energy conversion efficiency of thermoelectric generators for automobile systems where the heat sources are commonly cylindrical, a novel concentric annular thermoelectric generator (CATEG) consisting of annular thermocouples and a concentric annular heat exchanger is proposed. A numerical model of the CATEG is first established using a finite-element method, based on which the thermoelectric performances of the proposed CATEG and the conventional annular thermoelectric generator (ATEG) with a cylindrical heat exchanger are compared. The relationship between the size of the heat exchanger, heat transfer characteristics, and heat flow resistances are comprehensively studied. Furthermore, to balance the relationship between heat transmission and fluid flow resistances, and to extract the maximum net power, the optimal design of the concentric annular exchanger is obtained and analyzed. Simulation results show that the optimized ratio of the inner and outer diameters of the heat exchanger is 0.94, and the new ATEG with the proposed concentric annular heat exchanger can significantly increase the total heat transfer coefficient as well as the pressure drop, leading to a maximum net power of 65% higher than the conventional ATEG.

1. Introduction

Continuously improving the energy conversion efficiency of automobiles is one of the major pathways to conserve precious fossil energy sources and to reduce greenhouse gas emissions. In general, only 25% of fuel energy in the internal combustion engine vehicles is utilized for vehicle mobility and other necessary use, while about 30–40% is wasted as exhaust gas [1,2]. The wasted energy in the exhaust gas can be potentially recovered using a thermoelectric generator (TEG) by converting the heat into electric energy directly through thermoelectric effects. The thermal energy recovery TEG has attracted increasing research attention in recent years due to its advantages of simple and light-weighted structure, free of mechanical moving parts, high safety, and high reliability [3–5]. A typical TEG consists of a heat exchanger and many PN couples adhered to its surface [6]. However, the low conversion efficiency of the materials currently used for TEGs has limited their applications, while optimizing the TEG design is essential to improve its performance for practical applications and facilitate its commercialization process [7].

One of the causes of the low efficiency of the existing TEG design is that the temperature difference between the hot and the cold ends of the PN thermocouples is significantly smaller than that between the hot and the cold fluids [4]. Bell [8] pointed out that the reason for such a small temperature difference is the presence of large thermal resistance between the fluids and the thermocouples. Therefore, many researchers focus on enhancing the heat transfer characteristics to improve energy conversion efficiency [9]. The most common and most effective method to improve heat transmission characteristics is to put fillers in the exhaust channel of the hot-end exchanger with high thermal resistance. In order to improve the heat transmission rates and avert excessive back pressure, Wang et al. [10] investigated a hot side heat exchanger

* Corresponding author. School of Automation, Wuhan University of Technology, Wuhan, 430070, China.
E-mail address: jackxie@whut.edu.cn (C. Xie).
[1] W. Yang and W. Zhu contributed equally to this work.

https://doi.org/10.1016/j.energy.2021.122127
0360-5442/

Nomenclature

A	cross-sectional area of the exchanger, m^2
a_1,a_2,a_3	height, inner circular arc length and width of the PN couple, m
a_4	gap between *P*- and *N*-type legs, m
c	specific heat capacity, J g^{-1} K^{-1}
D_h	hydraulic diameter, m
d	convective heat transfer coefficient, W m^{-2} K^{-1}
dev	deviation percentage, %
F	Darcy resistance coefficient
H_r	surface roughness, m
h	height of heat exchanger, m
I	electric current, A
K	thermal conductance, W K^{-1}
k	total heat transfer coefficient, W m^{-2} K^{-1}
L	length of the heat exchanger, m
m	mass flow rate, g s^{-1}
n_x	total PN couple number in a line
n_r	total PN couple number in a single-ring
Nu	Nusselt number
P	power, W
p	pressure, Pa
Pr	Prandtl number
q	quantity of heat, W
R	resistance, Ω
Re	Reynolds number
r	radius, m
S	exchanger plate areas, m^2
T	temperature, °C
v	flow velocity, m s^{-1}

Superscript

i (j)	line (row) number
1	Case 1
2	Case 2

Greek

α	the Seebeck coefficient, V K^{-1}
δ	thickness, m
λ	thermal conductivity, W m^{-1} K^{-1}
ρ	density, kg m^{-3}; resistivity, Ω m
μ	dynamic viscosity, Pa s
η	efficiency, %
Δ	difference

Subscript

c	cold side of the thermocouple
cer	ceramic
con	connector
cu	copper
f	hot fluid
h	hot side of the thermocouple
i	inner ring of heat exchanger
L	external load
max	maximum value
n	*N*-type semiconductor
net	net value
opt	optimal value
p	*P*-type semiconductor
per	per unit module area
pn	thermocouple
$plate$	heat exchanger plate
$pump$	consumed pump value
teg	TEG module value
w	cold fluid

Abbreviations

ATEC	annular thermoelectric couple
ATEG	annular thermoelectric generator
TEG	thermoelectric generator
CATEG	concentric annular thermoelectric generator

with cylindrical grooves and studied the effects of three internal structures on the system through numerical simulation and evaluation of efficiency and net power. Kim et al. [11] fixed six 2-mm-thick plate fins on the hot surface of each thermoelectric module, and this method improved the heat transmission performance of TEG and increased the pressure drop on both sides of the pipe. Lu et al. [12] proved that by filling metal foam in the hot side exchanger channel, higher efficiency and power output can be achieved compared to using rectangular fins, whereas it leads to high back pressure and net power loss. In addition to enhancing the heat transfer performance of the heat exchanger, matching heat exchanger dimensions with the fluid characteristics and optimizing the structure of the thermoelectric module can also improve the efficiency of TEG [13,14]. For example, Fan et al. [15] developed a complete numerical model to compute the optimal size of thermocouples, and it was found that there exists an optimal leg length and an optimal cross-sectional area to achieve the maximum output power. Wang et al. [16] used a pitted surface to replace the inserted groove in the traditional heat exchanger. Compared with the heat exchanger with embedded pits, the new design effectively reduces the pressure drop and increases the net power. Niu et al. [17] studied the influences of gas channel size on thermoelectric performance. They found that a medium-sized heat exchanger should be used to balance the interaction between the pressure drop along the channel and the heat transmission.

Although considerable progress has been made on the flat-plate TEG (FTEG), such a design is not ideal for automobile exhaust gas heat recovery where the heat source, i.e., the exhaust pipe, is usually cylindrical [18]. The inherent geometric mismatch can cause the problems such as high energy loss and large heat transfer resistance, which would significantly reduce the performance of TEG. In recent years, with the advancements in material science and engineering, thermoelectric devices can be designed in various geometric shapes including annular thermocouples [19,20]. Unlike conventional flat-plate thermoelectric couple (FTEC), the cross-sectional area of an annular thermoelectric couple (ATEC) changes along the radial direction, and the contact resistance of an ATEC can be smaller than that of FTEC [21]. Shen et al. [22,23] proposed an annular thermoelectric generator (ATEG) and theoretically analyzed the influence of the leg's geometric characteristics on output power and efficiency under different temperature ratios and external loads. For cylindrical heat sources, an ATEG consisting of a cylindrical heat exchanger and many ATECs have been investigated in the literature. For example, Ge et al. [24] proposed a liquefied natural gas power generation system composed of an air-heated evaporator and a cylindrical ATEG, and a comprehensive comparison was provided in Ref. [25], in which the thermoelectric performances of ATEG and FTEG with cylindrical heat sources are analyzed from several aspects, including the convective heat transfer coefficient, inlet velocity, and temperature.

Although the abovementioned studies have been conducted to optimize the heat transfer capacity and efficiency of TEG, most of the existing investigations are based on traditional FTEGs, and the applicability of the obtained research outcomes and design guidelines from these works to ATEGs have not been examined. Regarding the numerical analysis and optimization of thermocouple design, recent research on TEG focused on components such as a single PN couple or segmented annular thermocouples for conventional design [26–28], whereas studies for structural improvement with novel designs at system levels is lacking, especially for the ATEG [29]. It is therefore not only beneficial but also necessary to investigate optimized structure to improve the energy efficiency of the whole system. In this connection, the major contributions and innovations of this paper are as follows:

1) A novel concentric annular thermoelectric generator (CATEG) composed of a concentric annular exchanger and ATECs is proposed for the first time.
2) A high-fidelity mathematical model of the CATEG is established. The model incorporates a thermal resistance network of CATEG considering temperature gradient, flow resistance, and heat transmission characteristics along the flow direction so that thermoelectric characteristics can be accurately predicted for performance evaluation and design improvement.
3) The thermoelectric characteristics and energy conversion performance of the CATEG system are analyzed comprehensively, and the range of the optimal design dimension for the concentric annular heat exchanger is obtained to achieve the maximum net power output.

The rest of the paper is structured as follows. A mathematical model of the CATEG is established in Section 2 for the present investigation. The proposed model is validated with simulation and experiment data in Section 3. The influences of dimensional parameters of the concentric annular heat exchanger on the thermoelectric performance are analyzed and the optimal design is obtained to maximize the net generated power of CATEG in Section 4. Conclusions are provided in Section 5.

2. Modeling of CATEG

2.1. Configuration and model assumptions

The CATEG system under investigation is shown in Fig. 1(a). It is composed of a concentric annular heat exchanger that carries the hot fluid of automobile exhaust gas, a coolant heat exchanger that carries the cold fluid, and many ring-shaped thermoelectric modules mounted in between. In the figure, h, r_i, and r denote the height, inner radius, and outer radius of the concentric annular heat exchanger, respectively, and L is the length of the CATEG/heat exchanger. The hot fluid heats the thermoelectric modules from one side (i.e., the hot end). A part of the thermal energy transferred to the modules is converted to electricity by the thermoelectric materials, and the rest energy is dissipated by the cold fluid via the other side of the modules (i.e., the cold end). The temperatures of the fluid entering the inlet of the concentric annular and coolant heat exchangers are denoted by T_{fin} and T_{win}, respectively.

Fig. 1(b) shows a non-isothermal finite-element model of the CATEG. The system is divided into $n_x \times n_r$ elementary units and each unit is denoted by (i, j) where i and j represent the indices of the row and the column, respectively. Each unit contains a thermocouple (i.e., a PN couple) which is composed of a p-type and an n-type semiconductor leg as shown in Fig. 1(c). The two legs are electrically connected in series with a copper connector and sandwiched between two identical ceramic sheets made of Al_2O_3, and all PN couples are connected in series. In Fig. 1(c), a_1, a_2, and a_3 are the height, inner circular arc length, and width of p-type or n-type legs, respectively, and a_4 is the gap between the legs. The radius corresponding to the inner circular arc length is denoted by r_{pn}, and the thicknesses of the copper connector and the ceramic sheet are denoted by δ_{cu} and δ_{cer}, respectively. The ceramic sheet functions as an electrically insulating layer which is essential for achieving heat transmission from the external thermal energy to the cooling components. The thickness of the exhaust heat exchanger and coolant heat exchanger tube wall is denoted as δ_{plate}.

An equivalent thermal resistance network, shown in Fig. 1(d), can be used to model and explain the heat transmission process in one elementary unit. In the ith row, the temperatures of the hot and the cold ends of the leg are denoted by T_h^i and T_c^i, respectively. On the one hand, as hot fluid flows through the calculation units, the temperature of the hot fluid will drop from T_f^i to T_f^{i+1}. On the other hand, the temperature of cold fluid rises from $T_w{}^i$ to $T_w{}^{i+1}$ when the cold fluid flows through the unit. When the thermal energy released by the engine exhaust is transferred to the ATEM, the total thermal resistance mainly consists of four components. From the inside to the outside, they are the convective heat transfer resistance, R_{f1}, the heat transfer resistance across concentric annular exchanger, R_{f2}, the thermal contact resistance between the surface of the heat exchanger and ATEM, R_{fcon}, and heat transfer resistance across the ceramic sheet and the copper connector, R_{f3}. Correspondingly, thermal resistances of the cold end are expressed as R_{w1}, R_{w2}, R_{wcon}, and R_{w3}, respectively. Assuming that there is no air between all PN legs, heat radiation and the Thomson effect can thus be ignored.

2.2. Mathematical model

As the fluid flows through the annular heat exchanger, the temperature of the thermocouple in the same ring is the same, so each calculation unit is marked by superscript i. For these calculation units, due to the heat conduction, two heat transfer components $q_h{}^i$ and $q_c{}^i$ are generated, which can be described by three sets of heat transfer equations. The first group is obtained by the temperature difference between fluid and thermoelectric device surface and is given by Newton's heat transfer law. The second group is the heat transfer equation considering the conduction heat, the Peltier effect and the Joule effect. The third group comes from the conservation of energy law, that is, the heat released by the fluid is equal to the heat absorbed by the thermoelectric module.

Based on the thermal resistance network and steady-state heat transmission process in a unit, it can be obtained and described by

$$\begin{cases} q_h^i = c_f m_f \left(T_f^i - T_f^{i+1}\right) \\ \quad = n_r \left[\alpha_{pn} I T_h^i + K_{pn}\left(T_h^i - T_c^i\right) - .0.5^2 R_{pn}\right] \\ \quad = n_r S_h k_f \left[0.5\left(T_f^i + T_f^{i+1}\right) - T_h^i\right] \\ q_c^i = c_w m_w \left(T_w^{i+1} - T_f^{i+1}\right) - T_h^i \\ \quad = n_r \left[\alpha_{pn} I T_c^i + K_{pn}\left(T_h^i - T_c^i\right) + 0.5 I^2 R_{pn}\right] \\ \quad = n_r S_c k_w \left[T_c^i - 0.5\left(T_w^{i+1} + T_w^i\right)\right] \end{cases} \tag{1}$$

where $q_h{}^i$ and $q_c{}^i$ are the heat absorbed at the hot side and the heat released at the cold side, and S_h and S_c represent the heat transmission areas of the hot and the cold ends, respectively. m_f and m_w are the mass flow rates of the hot fluid and the cold fluid, respectively. k_f and k_w are the total heat transfer coefficients of the heat transferred from hot fluid and cold fluid to the surface of the

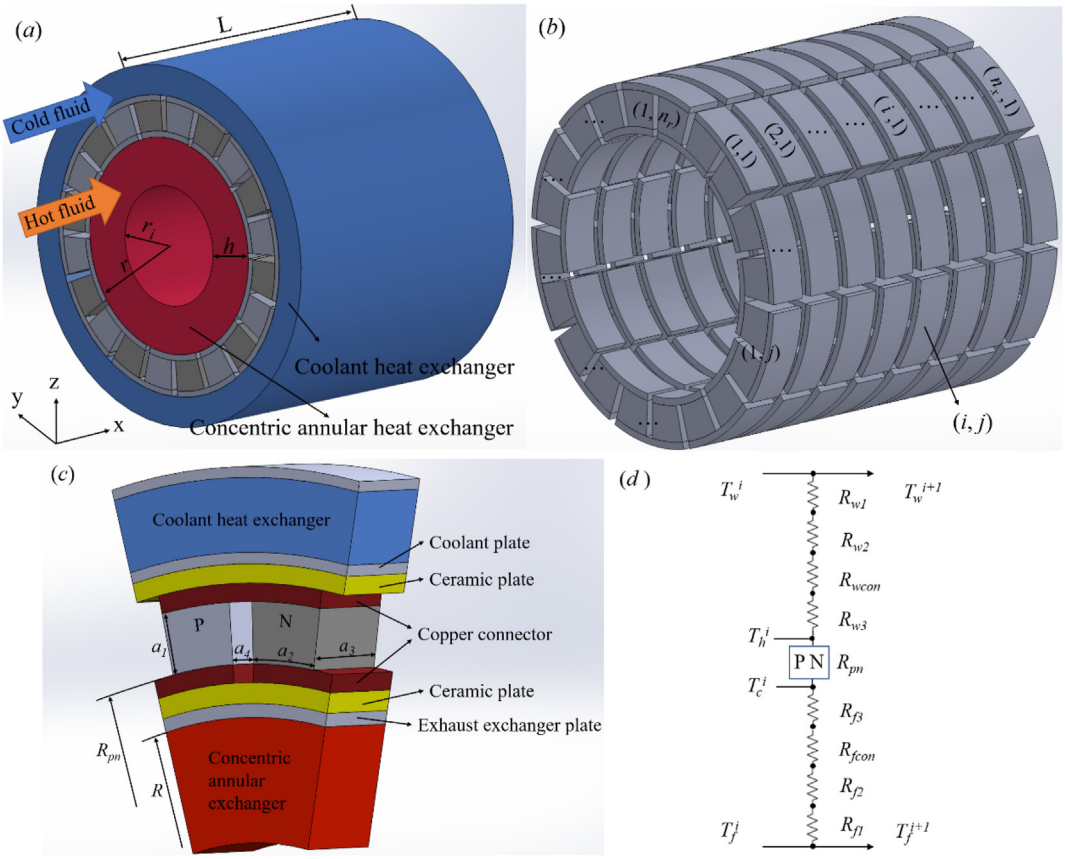

Fig. 1. Modeling of CATEG: (a) 3D view, (b) Finite element model, (c) 3D view of an elementary unit, (d) Equivalent thermal resistance network of an elementary unit.

thermoelectric element, and c_f and c_w are the specific heat capacities for the hot fluid and the cold fluid, respectively. In addition, α_{pn}, K_{pn}, and R_{pn} denote the Seebeck coefficient, thermal conductance, and electrical resistance of a PN couple, respectively, and they are determined by

$$\alpha_{pn} = \alpha_p - \alpha_n \tag{2}$$

$$K_{pn} = a_2 a_3 (\lambda_p + \lambda_p) / \{r_{pn} In[(r_{pn} + a_1) / r_{pn}]\} \tag{3}$$

$$R_{pn} = r_{pn} In[(r_{pn} + a_1) / r_{pn}] (\rho_p + \rho_n) / a_2 a_3 \tag{4}$$

where the symbols α, λ, and ρ represent the Seebeck coefficient, electrical resistivity, and thermal conductivity, respectively, while the subscripts "p" and "n" are attached to the symbols to represent the corresponding quantities for the p- and n-type legs, respectively.

The total heat transfer coefficient k_f is calculated by

$$\begin{aligned} k_f &= 1 \Big/ \left(R_{f1} + R_{f2} + R_{fcon} + R_{f3}\right) \\ &= 1 \Big/ \left(1 \Big/ d_f + \delta_{plate} \Big/ \lambda_{plate} + R_{fcon} + \delta_{cu} \Big/ \lambda_{cu} + \delta_{cer} \Big/ \lambda_{cer}\right) \end{aligned} \tag{5}$$

where λ_{plate}, λ_{cu}, and λ_{cer} represent the thermal conductivities of the heat exchanger wall, the copper connector, and the ceramic sheets, respectively. d_f is the convective heat transfer coefficient of hot fluid, obtained by

$$d_f = Nu \lambda_f \Big/ D_h \tag{6}$$

where λ_f is the thermal conductivity of the hot fluid, and D_h is the annulus hydraulic diameter defined as the difference between the outer and the inner diameters of the annulus.

In (6), the Nusselt number is determined by Ref. [30].

$$\begin{aligned} Nu = 0.0214 \left(\mathrm{Re}^{0.8} - 100\right) \mathrm{Pr}^{0.4} \Big[1 + (D_h/L)^{2/3} \left(T_{fav} \Big/ T_{wav}\right)^{0.45}, \\ 2300 \le \mathrm{Re} \le 10^6\Big] \end{aligned} \tag{7}$$

where Re and Pr are the Reynolds number and the Prandtl number of the hot fluid, respectively. T_{fav} and T_{wav} are the average temperatures of the hot fluid and the engine water in the fluid-flow direction, respectively. The Reynolds number can be calculated by

$$\mathrm{Re} = \rho_f D_h v_f \Big/ \mu_f \tag{8}$$

where ρ_f, v_f, and μ_f represent the density, velocity, and dynamic viscosity of the hot fluid, respectively.

Next, the fluid flow resistance characteristic of the hot side heat exchanger can be investigated by calculating the pressure drop Δp of the exhaust gas, i.e. [31],

$$\Delta p = 4F(L / D_h) \left(v_f^2 \rho_f \Big/ 2\right) \tag{9}$$

$$\begin{cases} F = \dfrac{0.0791}{\mathrm{Re}^{0.25}}, & 2000 < \mathrm{Re} \le \dfrac{59.7}{(2H_r/D_h)^{8/7}} \\ \dfrac{0.5}{\sqrt{F}} = -1.8\lg\left(\dfrac{6.8}{\mathrm{Re}} + \left(\dfrac{H_r}{3.7D_h}\right)^{1.11}\right), & \dfrac{59.7}{(2H_r/D_h)^{8/7}} < \mathrm{Re} \le 665 - \dfrac{765\lg(2H_r/D_h)}{2H_r/D_h} \\ F = \dfrac{0.25}{\left(2\lg\left(\dfrac{3.7D_h}{2H_r/D_h}\right)\right)^{2,}} & \mathrm{Re} > 665 - \dfrac{7651g(2H_r/D_h)}{2H_r/D_h} \end{cases} \tag{10}$$

Here, F is the Darcy resistance coefficient, determined by Ref. [32].

where H_r is the internal surface roughness of the heat exchanger.

Considering the pumping power loss due to gas resistance through the channel, it can thus be obtained by

$$P_{pump} = \Delta p\left(m_f \,/\, \rho_f\right) \tag{11}$$

Finally, the current I, output power P_{teg}, net power P_{net}, and efficiency η of the CATEG system are evaluated as follows,

$$I = \sum_{i=1}^{n_x} \alpha_{pn}\left(T_h^i - T_c^i\right) \,/\, \left(R_L + R_{pn} n_x n_r\right) \tag{12}$$

$$P_{teg} = \sum_{i=1}^{n_x}\left(q_h^i - q_c^i\right) \tag{13}$$

$$P_{net} = P_{teg} - P_{pump} \tag{14}$$

$$\eta = P_{net} \,/\, \sum_{i=1}^{n_x} q_h^i \tag{15}$$

2.3. Solution method

Given the model parameters, load resistance R_L, and boundary values T_{fin} and T_{win}, the developed model (1)–(15) shall be solved to obtain the current I (which equals the currents in all the PN couples) as well as the temperature distribution T^i of the CATEG system. However, since the current I and the temperatures are algebraically coupled by the highly nonlinear equations (1) and (12), the analytical solution cannot be obtained. The problem becomes more difficult as a similar coupling relationship exists between the temperature distribution of TEG and the convective heat transfer coefficient k_f as shown in (1) and (6). Hence, a numerical method with double iteration loops is proposed to efficiently solve the model, and the flowchart of the procedure is shown in Fig. 2.

The solution procedure is initialized with the initial guess I_0 and k_{f0} with which the initial temperature distribution is obtained by solving (1). According to the obtained temperature distribution, k_f can be updated using (6) and it is used as the new k_{f0} for the next iteration in the inner loop. The process is repeated until the convective heat transfer coefficient k_f is considered close enough to the previous inner iteration. Next, a new current I can be determined using (12), and the current is used as the new I_0 for the next iteration in the outer loop. The process is repeated until the current I is considered close enough to the previous outer iteration. Once I, k_f, and temperature distribution have been determined, the performance indicators of the TEG can be calculated using (13)–(15).

3. Model validation

3.1. Numerical and experimental validation

In the previous section, an accurate numerical model of CATEG is established with the consideration of the effects of ceramic plate, copper connector, and exchanger plate on the system. The model will be validated in this section by comparing the simulated results with the numerical and experimental results from the literature.

First, the simulation result of the proposed model is compared with the numerical data given in Ref. [33], where an ATEG with a hot-side cylindrical heat exchange channel was proposed and calculated net power output of the system for the loss of pumping power due to fluid resistance. In order to reproduce the data, we used the same parameters as given in Ref. [33] and set the inner radius r_i of the concentric annular heat exchanger to 0. By this means, the CATEG is equivalent to a conventional ATEG with a cylindrical heat exchanger. The maximum net powers of ATEG with different exhaust gas mass flow rates are shown in Fig. 3(a). It is observed that the maximum absolute error between the simulated result and data in Ref. [33] is 3.9%. This error is due to the consideration of the copper plate, ceramic sheets, and contact thermal

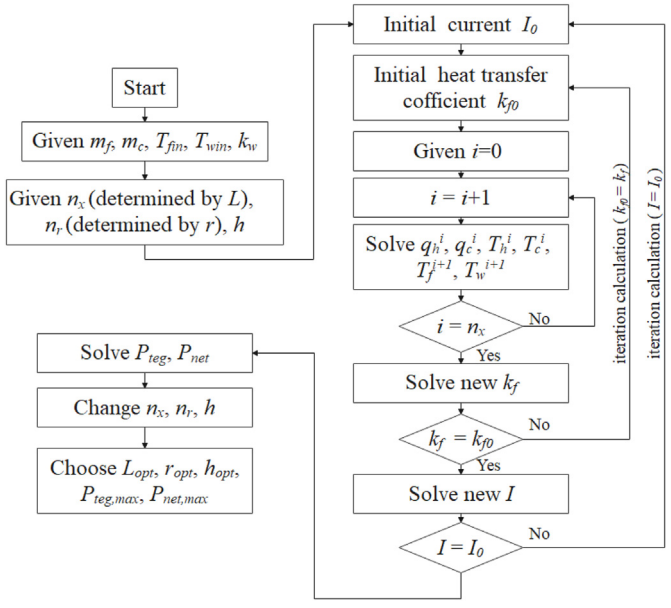

Fig. 2. Flowchart of the solution procedure.

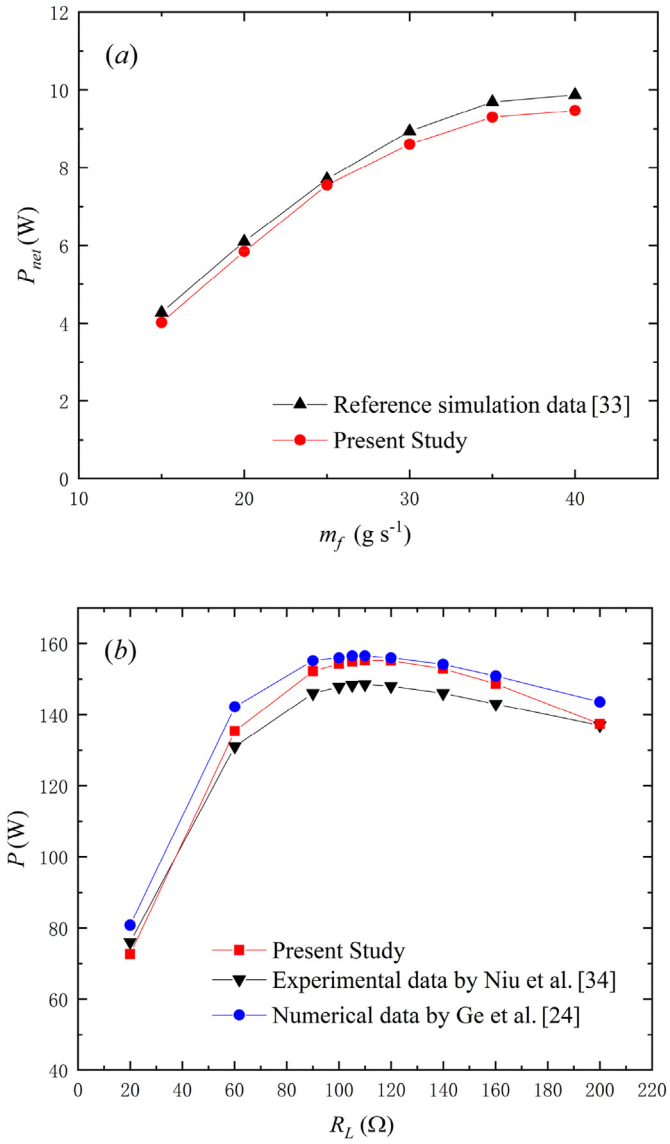

Fig. 3. Verification of the proposed arithmetic model. (a) Comparison with numerical results from Ref. [33]. (b) Comparison with experimental results from Ref. [34] and numerical results from Ref. [24].

resistance in our model.

For further validation of the proposed model, we compare the simulation result with experimental data extracted from the works by Niu et al. [34] and Ge et al. [24]. In this case, we consider the fact that when the radius of the ATEG is large enough, the curvature corresponding to the inner arc circular of the PN couple is small, and the annular thermoelectric couples can be regarded as FTECs. In the experiment, a commercial Bi_2Te_3 thermoelectric module with the dimensions of 40 mm × 40 mm × 4.2 mm was used. The average thermal conductivity, resistivity, and the Seebeck coefficient of the thermoelectric module are 1.7 W/(m·K), 9.5×10^{-6} Ω m, and 2×10^{-4} V/K, respectively, all measured at room temperature. We use the same parameters in our proposed model for model validation. The variation of power with different loads are shown in Fig. 3(b), and it is observed that the error between the predicted results from Ref. [24] and the experimental data was less than 10%, while the error between the proposed model and the experimental data is less than 8%, since the effects of ceramic plate, copper connector, and exchanger plate are considered in our model.

The proposed model structure is general, although the presented simulation results still exhibit some errors compared to the experimental results, and this is mainly due to the limitation in the model parameters. First, the parameters regarding the physical characteristics of the PN couples are set to constant, while in practice they are highly temperature-dependent. Second, the thermal contact resistance is set as 0.0008 m^2 K/W in the simulation, obtained from Ref. [30], while the true value for the experiment is not known. Furthermore, statistical approaches are beneficial for further model evaluation by considering the design uncertainties [35].

3.2. Performance analysis of the theoretical model

In addition, for further model comparison, Table 1 summarizes several prevailing modeling methods for the thermocouples or TEGs in the literature. It can be seen that many theoretical models of thermocouples or thermoelectric generators have been established using various modeling methods and implemented in different software, from one-dimensional to three-dimensional models and from analogy model to the thermal-electric numerical model. However, when the annular thermoelectric module is used to recover fluid waste thermal energy, especially the waste heat of automobile exhaust, few ATEG models can be adopted to comprehensively evaluate and optimize the thermoelectric and output performances of the ATEG system. For example, Ref. [22] established the mathematical model of the annular thermocouple using the finite element method, but when multiple thermocouples are coupled together to form a thermoelectric generator (TEG), accurate thermoelectric performance cannot be obtained. Ref. [24] established a numerical model of ATEG by constructing a thermal resistance network model, but the power loss caused by fluid resistance was not considered. Ref. [38] established a three-dimensional model of an ATEG through thermal stress analysis, and optimized the number and geometric structure of thermocouples, but did not consider the impact of the annular heat exchanger on ATEG.

Compared to the existing TEG models as given in Table 1, the thermal resistance model established in this work is a fluid-thermo-electric multiphysics field coupling model, which comprehensively considers the temperature gradient, flow resistance, and heat transmission characteristics along the flow direction. The model can accurately predict the thermoelectric performance and net power characteristics of CATEG by establishing a thermal resistance network model and iterative algorithms, the method can be generalized to provide guidelines for modeling new ATEG systems in the future.

4. Results and discussion

In this section, the effects of various design factors on thermoelectric performance, such as output power, net power, heat transfer performance, efficiency, etc., will be analyzed via simulation studies based on the validated CATEG model developed in the previous sections. The physical parameters of thermoelectric material (Bi_2Te_3) and the dimensions of the ATEC are presented in Table 2. In the automobile coolant system, the mass flow rate and the temperature are mw = 425 g/s and Twin = 70 °C [39], respectively. The contact thermal resistance is set to 0.0008 m^2·K/W. In addition, the thickness and the thermal conductivity of the ceramic sheet, the copper sheet, and the heat exchanger plate have significant influences on the heat transfer performance of the TEG, and they need to be determined according to practical situations. The basic parameters of heat source and TEG used in this work are

Table 1
Recent advances in modeling methods for TEC and TEG.

Research subject	Modeling Method and Software	Feature	Model Type	Ref.
TEC	Numerical model/MATLAB	1-D short calculation time	Thermal resistance model	[13]
	Finite-element method/MATLAB	1-D steady model	Thermal-electric numerical model	[22]
	ANSYS/EES	1-D short calculation time	Thermal resistance model	[36]
	SPICE/Mathematica	1-D steady-state analysis and analogies	Analogy model	[37]
TEG	Numerical simulation/MATLAB	from 1-D to 2-D iterative calculation	Thermal resistance model	[24]
	Numerical simulation/Fortran program	2-D iterative calculation	Thermal-electric numerical model	[30]
	Finite element approach/ANSYS	3-D steady-state	Thermal stress analyses	[38]

Table 2
Main physical and dimensional parameters of ATEC [39].

Parameters	Description	Value	Units
$a_1/a_2/a_3$	P(N)-type leg height/width/inner arc circular length	5/5/5	mm
a_4	Clearance between *P*-type and *N*-type legs	0.1	mm
α_p	*P*-type Seebeck coefficient	2.037×10^{-4}	V/K
α_n	*N*-type Seebeck coefficient	-1.721×10^{-4}	V/K
λ_p	*P*-type thermal conductivity	1.265	W/(m·K)
λ_n	*N*-type thermal conductivity	1.011	W/(m·K)
ρ_p	*P*-type resistivity	1.314×10^{-5}	Ω·m
ρ_n	*N*-type resistivity	1.119×10^{-5}	Ω·m

Table 3
Basic parameters of heat source and TEG.

Parameter	Description	Value	Unit
k_w	Heat transfer coefficient of water [30]	1000	W/(m^2·K)
T_{fin}	Exhaust gas inlet temperature	500	°C
T_{win}	Cooling water inlet temperature [39]	70	°C
m_f	Mass flow rate of exhaust gas	50	g/s
m_w	Mass flow rate of water [39]	425	g/s
R_{con}	Contact thermal resistance [30]	0.0008	m^2·K/W
δ_{cer}	Thickness of ceramic plate	0.05	mm
λ_{cer}	Thermal conductivity coefficient of ceramic plate	35	W/(m·K)
δ_{cu}	Thickness of copper connector	0.2	mm
λ_{cu}	Thermal conductivity coefficient of copper connector	398	W/(m·K)
δ_{plate}	Thickness of exchanger plate	0.3	mm
λ_{plate}	Thermal conductivity coefficient of exchanger plate	398	W/(m·K)

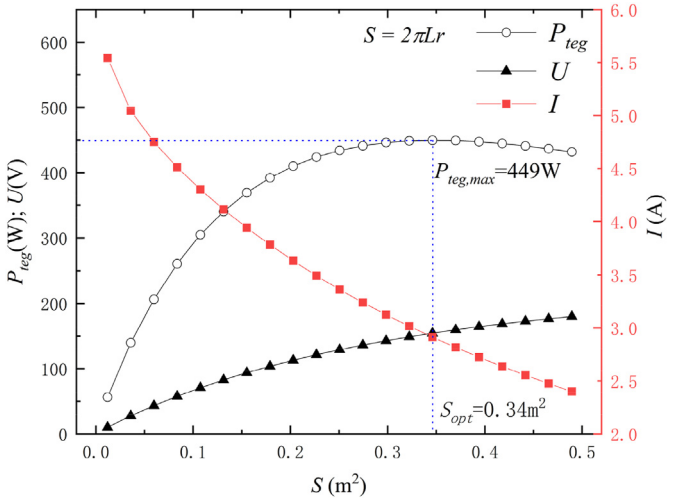

Fig. 4. Variations of P_{teg}, U, and I with S for $h = 5$ mm, $n_r = 20$.

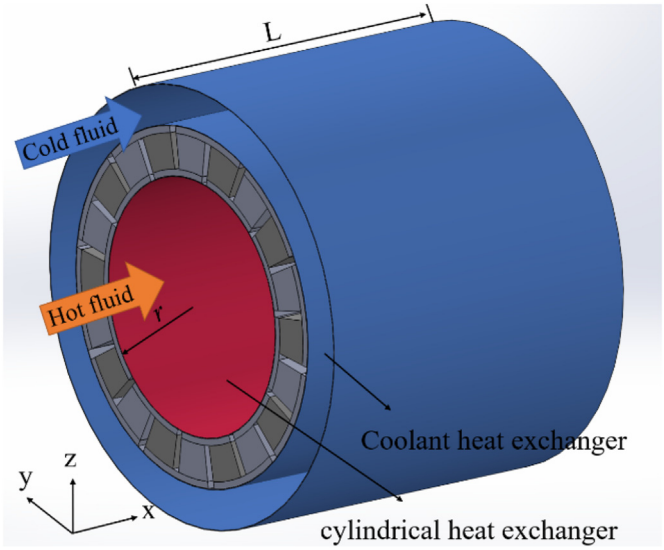

Fig. 5. Schematic diagram of the conventional cylindrical heat exchanger ATEG system.

provided in Table 3.

4.1. Thermoelectric performance analysis of CATEG

Fig. 4 shows the output power P_{teg}, voltage U, and current I of the CATEG as functions of the module area S. Here, the height of the exchanger h is set as 5 mm. The outer radius r of the concentric annular heat exchanger is 38 mm for an ordinary automobile exhaust pipe, and the corresponding number of units per module is $n_r = 20$. It can be seen that I reduces and U increases monotonously as S increases, while both of their rates of change decrease. Most importantly, there exists a maximum output power $P_{teg,max}$ for the CATEG. This is because, with an increased number of PN couples, the heat transfer area from the hot end to the cold end increases, the thermal resistance decreases, the heat conduction through the PN couples increases, and it results in a decrease in the output power. This result is also identified by He et al. [40]. Hence, for given parameters of the heat source, there exists an optimal module area S_{opt} to maximize P_{teg}. According to Fig. 4, when $S = S_{opt} = 0.34$ m^2, $P_{teg} = P_{teg,max} = 449$ W.

Next, we compare the thermoelectric characteristics of the CATEG with the conventional cylindrical heat exchanger ATEG equipped with the cylindrical heat exchanger. The mathematical model of the conventional ATEG was established based on the schematic diagram shown in Fig. 5, and its parameters are selected to be the same as the CATEG. Fig. 6(a) shows the influence of the length L of CATEG on output power, net power, and efficiencies for these two exhaust heat exchanger structures. It is observed that for the conventional cylindrical heat exchanger (Case 2), the difference between the net power P_{net} and the output power P_{teg} is small due to that the required pumping power is low. On the other hand, for the concentric annular heat exchanger (Case 1), although more pumping power is needed, the output power is higher than Case 2. The reason for this is because with the concentric heat exchanger, the heat transmission capacity of the hot side channel is increased and more thermal energy can be converted into electricity by the thermocouples. Fig. 6(b) shows the influence of L on pressure drop and heat transfer coefficient. It shows that, compared to the cylindrical heat exchanger, the concentric design can significantly improve the heat transfer coefficient, thereby increasing the output power. However, a higher pressure drop will also cause a higher pumping power consumption. According to Fig. 6(a), the net power of the CATEG is higher than the cylindrical design when $L < 2$ m,

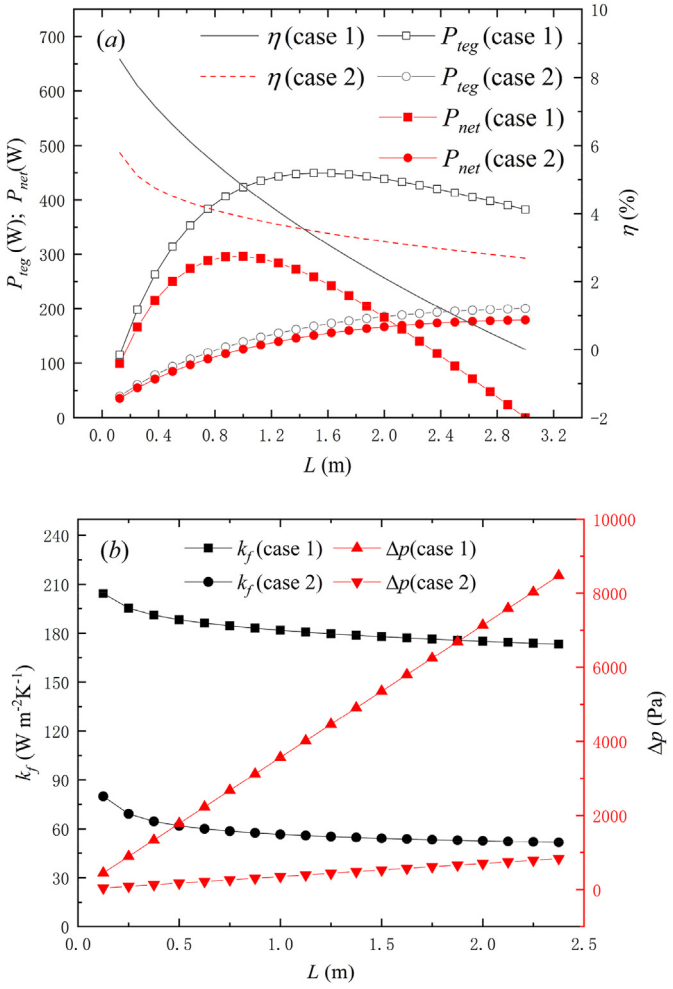

Fig. 6. Variations of (a) P_{teg}, P_{net}, η, (b) k_f, Δp with L for the same boundary condition (Case 1: concentric annular heat exchanger ATEG; Case 2: cylindrical heat exchanger ATEG).

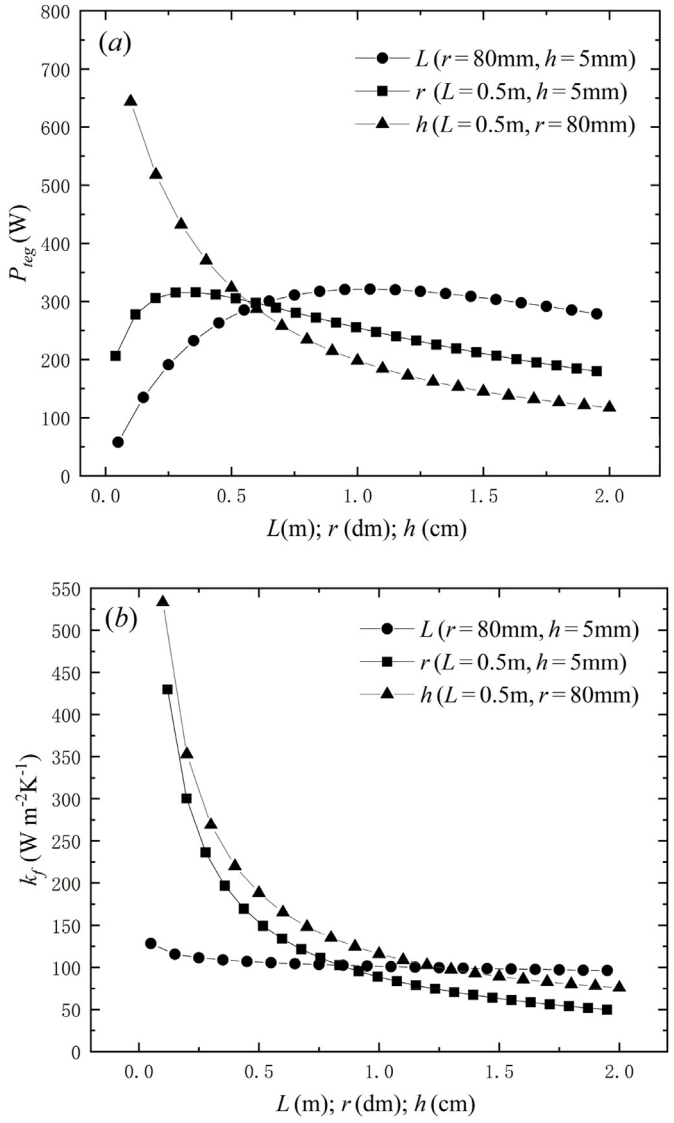

Fig. 7. CATEG power output and heat transfer coefficient versus exchanger height, radius, and length under the condition of stable heat source: (a) Output power; (b) Total heat transfer coefficient.

and the maximum net power of the CATEG is 65% higher than that of the cylindrical heat exchanger ATEG. When the peak net power is obtained, the efficiency of the CATEG is 4.7%. In addition, the new type of heat exchanger can be readily adapted according to the shape of the exhaust pipe, which can optimize the heat transfer characteristics, improve the heat transfer performance, and accommodate more ATECs. Therefore, the ATEG based on the concentric annular heat exchanger proposed in this paper is superior to the conventional cylindrical heat exchanger ATEG for automobile applications.

4.2. CATEG power output analysis based on fluid heat transfer characteristics

In this subsection, the influence of the dimension (L, r, and h) of the concentric annular heat exchanger on the heat transmission characteristics and output power of the CATEG will be discussed. The influence of dimension on P_{teg} with different design are shown in Fig. 7(a). It can be seen that in order to increase P_{teg}, it requires to reduce h or r, while an optimal heat exchanger length exists to obtain the maximum output power. This characteristic can be explained using Fig. 7(b), where it shows that the heat transfer coefficient k_f will reduce when L, r, or h increases. However, since the cross-sectional area A is the major factor affecting k_f, according to $A = \pi r^2 - \pi(r-h)^2$, changing L is less effective compared with changing r or h, as can be observed from Fig. 7(b).

Next, with A increases, the maximum output power $P_{teg,max}$, the optimal module area S_{opt}, corresponding optimal total heat transfer coefficient can be obtained and the relationships are shown in Fig. 8. It can be seen that reducing A can increase $P_{teg,max}$ as well as the corresponding $k_{f,opt}$, while the corresponding S_{opt} will decrease almost linearly as A reduces. In this case, when the cross-sectional area is $A = 0.0011$ m^2, the maximum power $P_{teg,max} = 449$ W is obtained, which is the same as that given in Fig. 4. The corresponding optimal module area $S_{opt} = 0.36$ m^2 and the optimal total heat transfer coefficient $k_{f,opt} = 177$ W m^{-2} K^{-1}.

In addition, we show in Fig. 9 that radius r and height h have significant influences on the optimal module length L_{opt}. It can be seen that L_{opt} has a positive correlation with height h, and this relationship is similar to that between A and S_{opt} as shown in Fig. 8. Therefore, in order to obtain a smaller L, the heat exchanger should be designed with a smaller h and/or a larger r.

When the cross-sectional area $A = 0.0011$ m^2, Fig. 10 shows the influence of h on L_{opt}, S_{opt}, r, $P_{teg,max}$, and $k_{f,opt}$. From Fig. 10(a), it can be seen that L_{opt} increases approximately linearly as h increases, while h has a negligible effect on S_{opt}. From Fig. 10(b), both $P_{teg,max}$ and the corresponding $k_{f,opt}$ decrease with the increase of h.

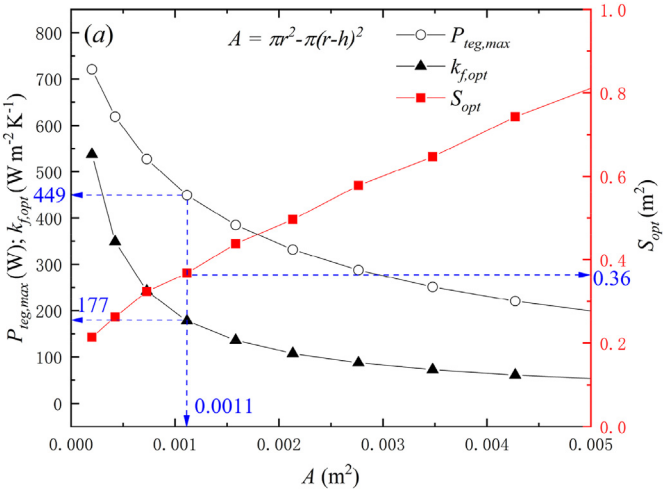

Fig. 8. Variations of $P_{teg,max}$, $k_{f,opt}$, and S_{opt} with different A.

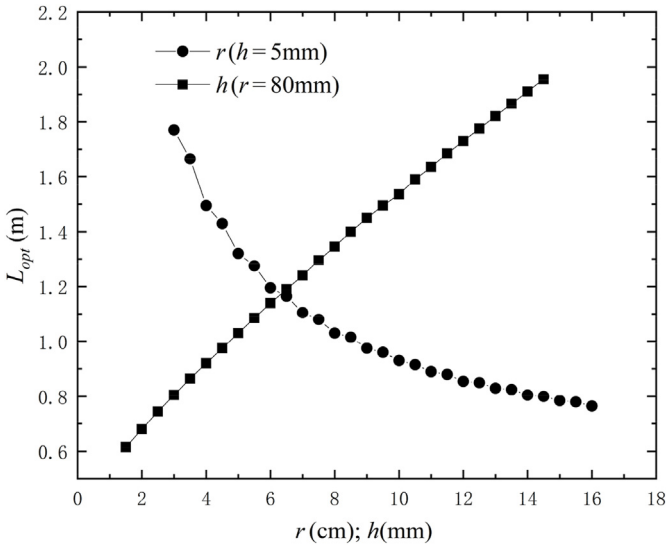

Fig. 9. Variations of L_{opt} with different r and h.

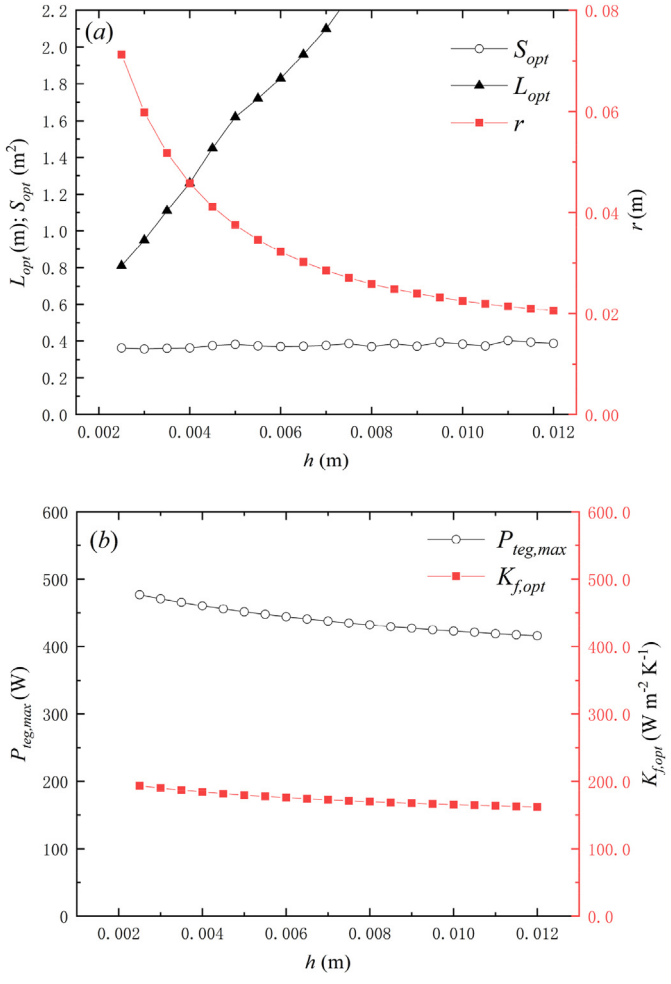

Fig. 10. Variations of (a) L_{opt}, S_{opt}, r, (b) $P_{net,max}$, and $k_{f,opt}$ with h for $A = 0.0011$ m^2.

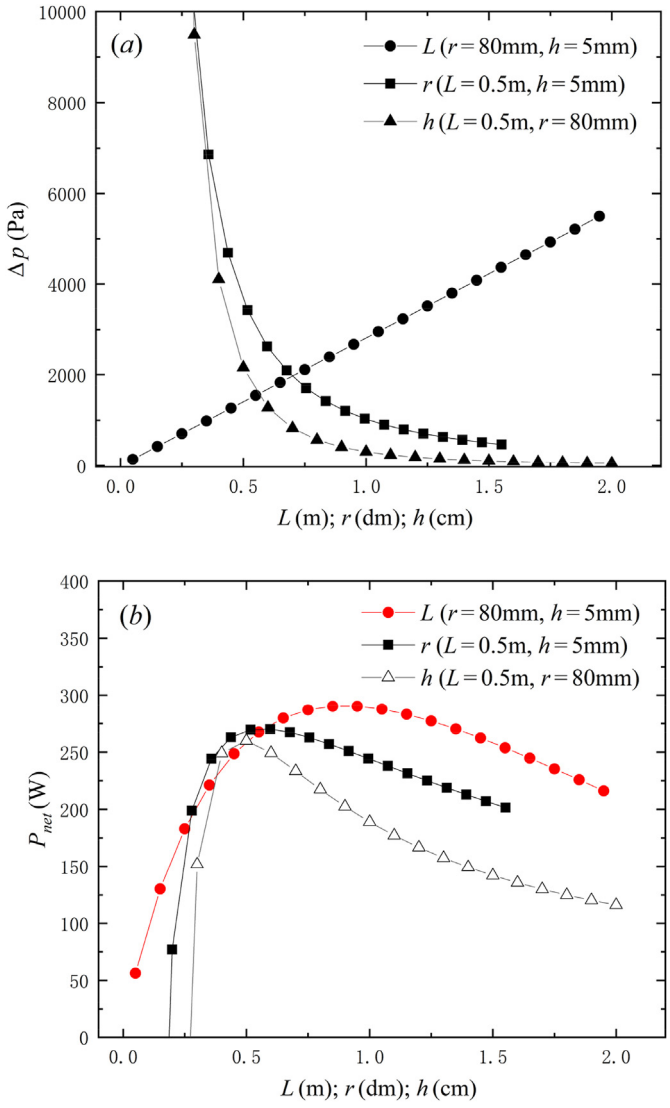

Fig. 11. Relationship between (a) pressure drop, (b) net power, and exchanger sizes (length, radius, and height).

Therefore, when the cross-sectional area of the heat exchanger is fixed, a smaller height can be selected to obtain a higher output power and a smaller module area.

4.3. CATEG net power analysis based on flow resistance characteristics

According to the results obtained in the previous subsections, one shall reduce the cross-sectional area A to increase the output power of the CATEG. However, a smaller A will also cause larger heat flow resistances, which can lead to additional pump power consumption. Such a design trade-off will be analyzed in this subsection.

Fig. 11 shows the change in pressure drop Δp as well as net power P_{net} with various exchanger dimensions. It can be seen from Fig. 11(a) that, Δp decreases significantly as h or r increases, while it increases as the L increases almost linearly. Fig. 11(b) shows that there exists an optimal design for h, r, and L to achieve the maximum P_{net}, and this is different from the case as shown in Fig. 7(a) where only L has an optimal value.

This can be explained with Fig. 7(b): A small h can lead to a large k_f and a large P_{teg}, whereas it will also increase Δp as well as P_{pump}. As h increases, Δp and P_{pump} gradually decrease, so P_{net} first increases to the maximum value and then gradually decreases. To obtain the optimal output characteristics, it is necessary to balance the two factors of heat transmission as well as fluid flow resistance, so an optimal heat exchanger height can be determined to maximize the net power.

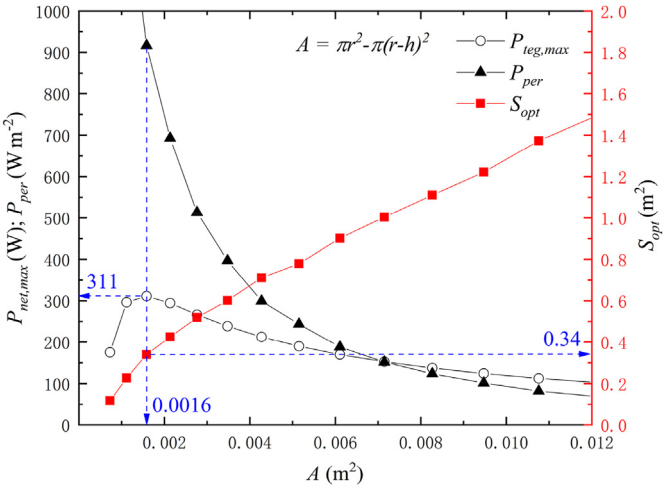

Fig. 12. Relationships of $P_{net,max}$, S_{opt}, and P_{per} versus A.

The cross-sectional area A also significantly affects the pressure drop Δp. The changes in the maximum net power output $P_{net,max}$, power per unit area P_{per}, and the corresponding module area S_{opt} with various A are shown in Fig. 12. It is observed that S_{opt} increases approximately linearly with the increase of A, similar to Fig. 8. In addition, $P_{net,max}$ first increases and then decreases as A increases. The peak $P_{net,max}$ is reached at $A = 0.0016$ m^2, and the corresponding P_{per} is high. The result is more practical than that shown in Fig. 8, since Fig. 8 indicates that a smaller A can always lead to a higher $P_{net,max}$.

Next, Fig. 13(a) shows the effect of height h on the optimal exchanger dimensions for the optimal cross-sectional area $A_{opt} = 0.0016$ m^2. From it, both the optimal length L_{opt} and the optimal module area S_{opt} increase linearly as h increases. When $h < 0.002$ m, $r_{opt} > 13$ cm; when $h > 0.01$ m, $L_{opt} > 2$ m. Therefore, the optimal height h_{opt} should be in the range of 0.002–0.01 m for automobile applications.

For the same $A_{opt} = 0.0016$ m^2, Fig. 13(b) illustrates the influence of h on the maximum net power, corresponding $k_{f,opt}$, and degree of net power deviation dev_{per}. Here, dev_{per} is defined as:

$$dev_{per} = 100 \times \left(P_{net,peak} - P_{net,\max}\right) \Big/ P_{net,peak} \tag{16}$$

It can be seen that in this case the changes in $k_{f,opt}$ and $P_{net,max}$ are small. When $h = 0.004$ m, $P_{net,\max}$ reaches the peak value, denoted by $P_{net,\,peak}$. Therefore, in this condition, the optimal design of heat exchanger is $h_{opt} = 0.004$ m, $r_{opt} = 0.066$ m, $L_{opt} = 0.77$ m, and $S_{opt} = 0.32$ m^2, and the corresponding optimal total heat transfer coefficient is $k_{f,opt} = 108$ W m^{-2} K^{-1}. In addition, $dev_{per} <$ 5.2% within the optimal heat exchanger height range of 2–10 mm when the optimum cross-sectional area A_{opt} is obtained.

In the FTEG, the heat exchanger is a thin cuboid channel with an optimal height of 5 mm, which ensures that the FTEG has improved heat transfer characteristics and increased power output [30]. In CATEG, the fluid channel is a similar thin concentric annular channel, the optimum height of the heat exchanger is 4 mm. This difference is due to the use of annular thermocouples and the

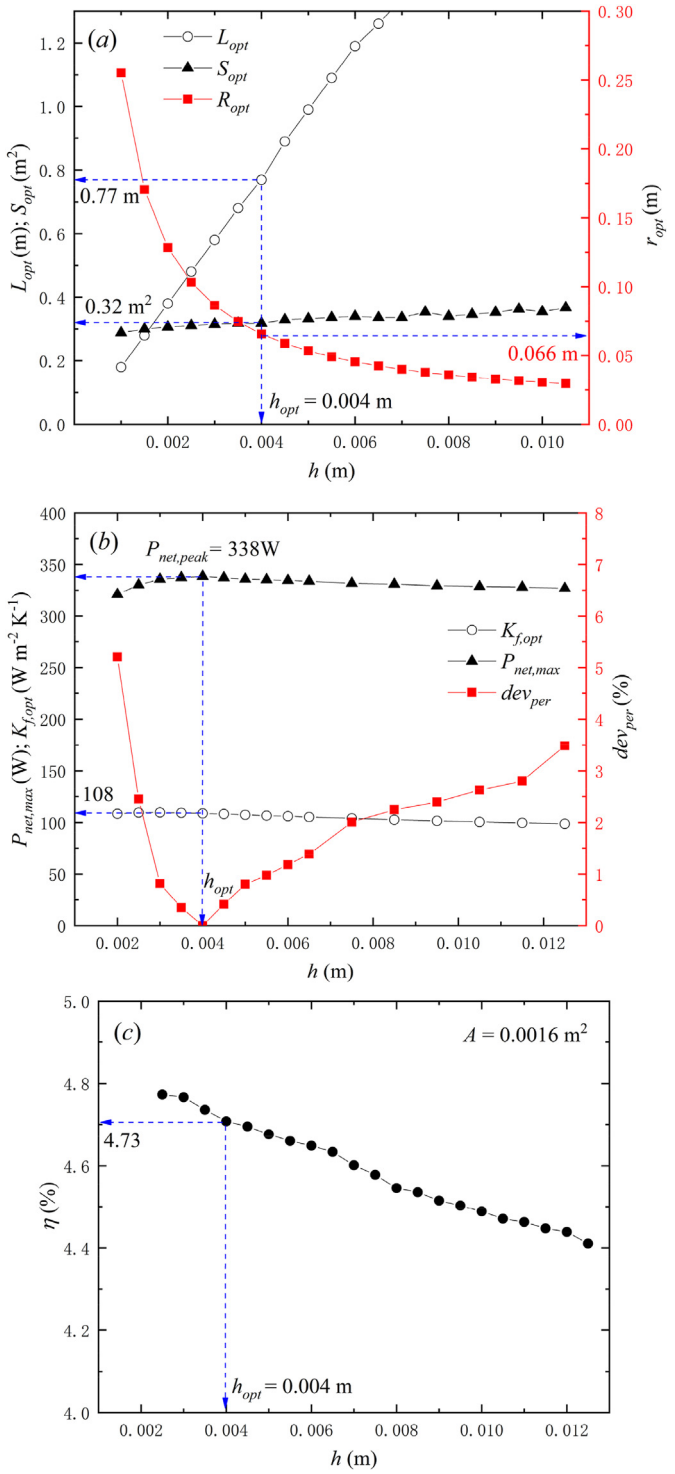

Fig. 13. Variations of (a) optimal heat exchanger dimension (length, radius, height, and module area), (b) net power, heat transfer coefficient, net power deviation, and (c) conversion efficiency with h.

unconventional structure of the heat exchanger. The optimal heat exchanger dimensions can be obtained using the design equations in the case of variable exhaust parameters in FTEG [41]. In the CATEG, the optimal size will also change with the parameters of the heat source. The optimum dimension design of concentric annular heat exchanger ATEG under stable operating conditions of automobiles is the focus of this paper, therefore, the optimization design of automobile ATEG system under variable operating conditions will be our future work.

The conversion efficiency η is obtained with different h, shown in Fig. 13(c). It can be observed that $\eta > 4.5\%$ within the optimal height range of 2–10 mm, and for the optimum height $h_{opt} = 0.004$ m, the efficiency is $\eta = 4.73\%$. Hence, with the optimal design as presented in Fig. 13(a), excellent performance of CATEG can be obtained in a wide range of selection of exchanger height.

To express the optimal height of the concentric annular heat exchanger more intuitively, dimensionless analysis is carried out by defining θ as the ratio of the inner diameter to outer diameter of the concentric annular heat exchanger:

$$\theta = r_i / r \tag{17}$$

The range of the optimal θ is found to be 0.85–0.97. When θ is 0.94, the maximum net power of 338 W can be reached.

5. Conclusions

In order to recover the exhaust thermal energy from automobile waste gas effectively, a new type of annular thermoelectric generator (ATEG) named the concentric annular heat exchanger ATEG (CATEG) is proposed in this paper. A comprehensive CATEG mathematical model is developed and the novel features of the proposed CATEG system are identified and analyzed. The main findings in this work are summarized as follows.

1) The concentric annular heat exchanger increases the total heat transfer coefficient, enhances the heat transmission capacity, and improves the output power of ATEG. Compared with the conventional cylindrical heat exchanger ATEG, the maximum net power of CATEG can be increased by 65%.
2) When designing a concentric heat exchanger for an ATEG, it is recommended to choose the dimensions with a small height h, a small length L, and a moderate radius r (See Fig. 1(a) for definitions). In addition, for a given cross-sectional area, the optimal length increases linearly with the increase of height of the heat exchanger, and a larger height corresponds to lower power output and a longer optimal module length.
3) According to the calculation conditions given in this paper, the peak net power can be obtained when the cross-sectional area of the heat exchanger is 0.0016 m^2. The optimal ratio of the inner diameter to outer diameter of the heat exchanger is 0.94, and the corresponding maximum net power is 338 W.
4) The recommended ratio of the inner diameter to outer diameter of the concentric annular heat exchanger is in the range of 0.85–0.97. Within this range, the maximum net power deviation can be limited below 5.2%, and the efficiency is higher than 4.5%.

Author contributions

Conceptualization, Changjun Xie, Bo Zhao and Liang Huang; Data curation, Wenlong Yang and Wenchao Zhu; Formal analysis, Leiqi Zhang and Yang Li; Funding acquisition, Changjun Xie and Yonggao Yan; Investigation, Wenchao Zhu and Yang Li; Methodology, Wenchao Zhu and Yonggao Yan; Project administration, Changjun Xie and Bo Zhao; Software, Liang Huang and Wenlong Yang; Supervision, Bo Zhao and Changjun Xie; Validation, Yonggao Yan and Leiqi Zhang; Writing – original draft, Wenlong Yang and Wenchao Zhu; Writing – review & editing, Changjun Xie and Yang Li.

Declaration of competing interest

The authors declare that they have no known competing financial interests or personal relationships that could have appeared to influence the work reported in this paper.

Acknowledgments

This research was supported by the National Natural Science Foundation of China (51977164), and the Wuhan Frontier Project on Applied Research Foundation (2019010701011405).

References

[1] Fan S, Gao Y. Numerical analysis on the segmented annular thermoelectric generator for waste heat recovery. Energy 2019;183:35–47.
[2] Li X, Xie C, Quan S, Huang L, Fang W. Energy management strategy of thermoelectric generation for localized air conditioners in commercial vehicles based on 48 V electrical system. Appl Energy 2018;231:887–900.
[3] Elghool A, Basrawi F, Ibrahim TK, Habib K, Ibrahim H, Idris DMND. A review on heat sink for thermo-electric power generation: classifications and parameters affecting performance. Energy Convers Manag 2017;134:260–77.
[4] Li Y, Xiong B, Vilathgamuwa DM, Wei Z, Xie C, Zou C. Constrained ensemble Kalman filter for distributed electrochemical state estimation of lithium-ion batteries. IEEE Trans. Ind. Informat. 2021;17(1):240–50.
[5] Zhao Y, Wang S, Ge M, Li Y, Liang Z, Yang Y. Performance analysis of a thermoelectric generator applied to wet flue gas waste heat recovery. Appl Energy 2018;228:2080–9.
[6] Li X, Xie C, Quan S, Shi Y, Tang Z. Optimization of thermoelectric modules' number and distribution pattern in an automotive exhaust thermoelectric generator. IEEE Access 2019;7:72143–57.
[7] Huang S, Xu X. A regenerative concept for thermoelectric power generation. Appl Energy 2017;185:119–25.
[8] Bell LE. Cooling, heating, generating power, and recovering waste heat with thermoelectric systems. Science 2008;321:1457–61.
[9] Vale S, Heber L, Coelho PJ, Silva CM. Parametric study of a thermoelectric generator system for exhaust gas energy recovery in diesel road freight transportation. Energy Convers Manag 2017;133:167–77.
[10] Wang Y, Li S, Zhang Y, Yang X, Deng Y, Su C. The influence of inner topology of exhaust heat exchanger and thermoelectric module distribution on the performance of automotive thermoelectric generator. Energy Convers Manag 2016;126:266–77.
[11] Kim TY, Lee S, Lee J. Fabrication of thermoelectric modules and heat transfer analysis on internal plate fin structures of a thermoelectric generator. Energy Convers Manag 2016;124:470–9.
[12] Lu C, Wang S, Chen C, Li Y. Effects of heat enhancement for exhaust heat exchanger on the performance of thermoelectric generator. Appl Therm Eng 2015;89:270–9.
[13] Tian H, Sun X, Jia Q, Liang X, Shu G, Wang X. Comparison and parameter optimization of a segmented thermoelectric generator by using the high temperature exhaust of a diesel engine. Energy 2015;84:121–30.
[14] Baker C, Vuppuluri P, Shi L, Hall M. Model of heat exchangers for waste heat recovery from diesel engine exhaust for thermoelectric power generation. J Electron Mater 2012;41:1290–7.
[15] Fan L, Zhang G, Wang R, Jiao K. A comprehensive and time-efficient model for determination of thermoelectric generator length and cross-section area. Energy Convers Manag 2016;122:85–94.
[16] Wang Y, Li S, Xie X, Deng Y, Liu X, Su C. Performance evaluation of an automotive thermoelectric generator with inserted fins or dimpled-surface hot heat exchanger. Appl Energy 2018;218:391–401.
[17] Niu Z, Diao H, Yu S. Investigation and design optimization of exhaust-based thermoelectric generator system for internal combustion engine. Energy Convers Manag 2014;85:85–101.
[18] Manikandan S, Kaushik SC. Energy and exergy analysis of solar heat pipe based annular thermoelectric generator system. Sol Energy 2016;135:569–77.
[19] Zhou X, Yan Y, Lu X, Zhu H, Han X, Chen G, Ren Z. Routes for high-performance thermoelectric materials, Mater. Today Off 2018;21(9):974–88.
[20] Blackburn JL, Ferguson AJ, Cho C, Grunlan JC. Carbon-nanotube-based thermoelectric materials and devices. Adv Mater 2018;30(11):1704386.
[21] Bauknecht A, Steinert T, Spengler C, Suck G. Analysis of annular thermoelectric couples with nonuniform temperature distribution by means of 3-D multiphysics simulation. J Electron Mater 2013;42:1641–6.
[22] Shen Z-G, Wu S-Y, Xiao L. Theoretical analysis on the performance of annular thermoelectric couple. Energy Convers Manag 2015;89:244–50.
[23] Shen Z-G, Wu S-Y, Xiao L. Assessment of the performance of annular thermoelectric couples under constant heatflux condition. Energy Convers Manag 2017;150:704–13.
[24] Ge M, Wang X, Zhao Y. Performance analysis of vaporizer tube with thermoelectric generator applied to cold energy recovery of liquefied natural gas. Energy Convers Manag 2019;200:112112.
[25] Zhang M, Wang J, Tian Y. Performance comparison of annular and flat-plate thermoelectric generators for cylindrical hot source. Energy Rep 2021;7:413–20.
[26] Zhang AB, Wang BL, Pang DD. Effects of interface layers on the performance of annular thermoelectric generators. Energy 2018;147:612–20.
[27] Shittu S, Li G, Zhao X. High performance and thermal stress analysis of a segmented annular thermoelectric generator. Energy Convers Manag 2019;184:180–93.
[28] Shen Z-G, Liu X, Chen S. Theoretical analysis on a segmented annular thermoelectric generator. Energy 2018;157:297–313.
[29] Hosseini M, Abdelrazek AH, Sadri R. Numerical study of turbulent heat transfer of nanofluids containing eco-friendly treated carbon nanotubes through a concentric annular heat exchanger. Int J Heat Mass Tran 2018;127:403–12.
[30] He W, Wang S, Li Y, Zhao Y. Structural size optimization on an exhaust exchanger based on the fluid heat transfer and flow resistance characteristics applied to an automotive thermoelectric generator. Energy Convers Manag 2016;129:240–9.
[31] Mavridou S, Mavropoulos GC, Bouris D, Hountalas DT, Bergerles G. Comparative design study of a diesel exhaust gas heat exchanger for truck applications with conventional and stage of the art heat transfer enhancements. Appl Therm Eng 2010;30:935–47.
[32] Cui H, Shi Z, Yang S, Yue X, Meng J. Engineering fluid mechanics. 1th ed. Beijing: Petroleum industry Press; 1995.
[33] Yang Y, Wang S, Zhu Y. Evaluation method for assessing heat transfer enhancement effect on performance improvement of thermoelectric generator systems. Appl Energy 2020;263:114688.
[34] Niu Z, Diao H, Yu S, Jiao K, Du Q, Shu G. Investigation and design optimization of exhaust-based thermoelectric generator system for internal combustion engine. Energy Convers Manag 2014;85:85–101.
[35] Ozgur MA, Arslan O, Kose R, Peker KO. Statistical evaluation of wind characteristics in kutahya, Turkey, energy sources Part A – recov. Util. Environ. Effects 2009;31:1450–63.
[36] Fraisse G, Ramousse J, Sgorlon D, Goupil C. Comparison of different modeling approaches for thermoelectric elements. Energy Convers Manag 2013;65:351–6.
[37] Mitrani D, Salazar J, Turó A, García MJ, Chávez JA. One-dimensional modeling of TE devices considering temperature-dependent parameters using SPICE. Microelectron J 2009;40:1398–405.
[38] Fan S, Gao Y. Numerical simulation on thermoelectric and mechanical performance of annular thermoelectric generator. Energy 2018;150:38–48.
[39] Jack TK, Ojapah MM. Water-cooled petrol engines: a review of considerations in cooling systems calculations with variable coolant density and specific heat. Int J Adv Eng Technol 2013;6:659–67.
[40] He W, Guo R, Liu S, Zhu K, Wang S. Temperature gradient characteristics and effect on optimal thermoelectric performance in exhaust power-generation systems. Appl Energy 2020;261:114366.
[41] He W, Guo R, Takasu H, Kato Y, Wang S. Performance optimization of common plate-type thermoelectric generator in vehicle exhaust power generation systems. Energy 2019;175:1153–63.